Numerical Heat Transfer, Part A: Applications: An International Journal of Computation and Methodology
Publication details, including instructions for authors and subscription information:
http://www.tandfonline.com/loi/unht20

TUMBLING/SQUISH INTERACTION IN LOOP-SCAVENGED TWO-STROKE ENGINES

Yeng-Yung Tsui [a] & Hong-Ping Cheng [a]
[a] Department of Mechanical Engineering , National Chiao Tung University , Hsinchu, Taiwan, Republic of China
Published online: 12 Mar 2007.

To cite this article: Yeng-Yung Tsui & Hong-Ping Cheng (1997) TUMBLING/SQUISH INTERACTION IN LOOP-SCAVENGED TWO-STROKE ENGINES, Numerical Heat Transfer, Part A: Applications: An International Journal of Computation and Methodology, 32:8, 861-876, DOI: 10.1080/10407789708913921

To link to this article: http://dx.doi.org/10.1080/10407789708913921

TUMBLING/SQUISH INTERACTION IN LOOP-SCAVENGED TWO-STROKE ENGINES

Yeng-Yung Tsui and Hong-Ping Cheng
Department of Mechanical Engineering, National Chiao Tung University, Hsinchu, Taiwan, Republic of China

This article describes a numerical investigation of the flow in a loop-scavenged two-stroke engine equipped with a head-bowl combustion chamber. The bowl is either placed in the center of the cylinder head or displaced away from the center. Attention is focused on the period of compression and early expansion. Results show that the effects of compression of the tumbling vortex by the piston become prominent after the midcompression stage, resulting in significant cascading of energy from mean flow to turbulence, followed by a fast decay of turbulence. The subsequent emergence of squish and reverse squish helps retard the decay. As a consequence, the cases with head bowls possess higher levels of mean flow and turbulence than those without bowls at top dead center and the later stage. It is also shown in the results that the offset of the head bowl has significant effects on the mean flow and turbulence characteristics, highly dependent on the offset direction.

INTRODUCTION

In high-speed internal combustion engines it is essential to have a strong bulk flow to generate sufficiently high turbulence in the late compression such that ignition can be successfully started and combustion can be completed quickly. To fulfill this objective, an usual means is to create a swirl, a flow rotating in the direction of the cylinder axis, during the intake stroke via a directed or helical port/valve assembly. The swirling flow may persist into the compression period. In direct-injection Diesel engines a combustion chamber of bowl shape is placed on the piston head. As top dead center (TDC) is approached, the air in the cylinder is forced into the piston bowl. As a consequence of the lower mean radius of gyration of the bowl, the rotational speed of this swirl is enhanced owing to conservation of angular momentum [1, 2]. Another prominent flow feature, termed "squish," appears at time near TDC because air in the clearance between the cylinder head and the piston crown rushes to flow into the bowl. A simple theory for calculation of the squish velocity, based on the instantaneous mass conservation law for the squish zone, was developed by Fitzgeorge and Allison [1]. In this model it is assumed that the squish flow is one-dimensional and the density is uniformly

Received 30 April 1997; accepted 13 August 1997.

The authors wish to acknowledge support provided by the National Science Council, Republic of China, under Contract Number NCHC 85-06-006. The authors are also indebted to the National Center for High-Performance Computing for providing computer resources.

Address correspondence to Dr. Y.-Y. Tsui, Department of Mechanical Engineering, National Chiao Tung University, Hsinchu 300, Taiwan, Republic of China.

Numerical Heat Transfer, Part A, 32:861–876, 1997

1040–7782/97 $12.00 + .00

NOMENCLATURE

A	area of the port opening	u, v, w	density-weighted ensemble-averaged velocities in the ξ, η, and ζ directions, respectively
ATDC	after top dead center		
BTDC	before top dead center		
CA	crank angle	$\bar{V}_P$	mean piston speed
C_D	discharge coefficient	$\hat{w}$	axial velocity relative to the moving-grid velocity
EPISO	engine application of PISO		
EPO	exhaust port opening	Γ_Φ	diffusion coefficient for Φ
k	turbulence kinetic energy	Δ	increment
$\dot{m}$	mass flow rate through cylinder port	ΔP	effective pressure difference
		ΔV	volume of considered cell
r, z, θ	radial, axial, and azimuthal directions, respectively	ϵ	turbulence dissipation rate
		ξ, η, ζ	curvilinear orthogonal coordinates
S	source term	ρ	density
t	time	Φ	density-weighted ensemble-averaged variable
TDC	top dead center		

distributed. Good agreement was obtained between the predictions by the simple theory and the multidimensional calculations of Gosman and Johns [3]. In the absence of swirl, a single torroidal vortex is created in the bowl during the late compression [3, 4]. With swirl, the penetration of the squish jet toward the bowl axis is reduced by the centrifugal force induced by the swirling motion, and the flow in the bowl becomes more complicated with the appearance of two or more vortices formed [3–5]. Turbulence is produced by the high shear stresses at the region around the bowl periphery. However, the overall turbulence levels remain comparable to those with the flat piston, as reported by Arcoumanis et al. [4], unless a reentrant bowl is incorporated.

Recently, a more effective way than the use of swirl to enhance turbulence has drawn much attention. It was reported in the study of Gosman et al. [6] that a tumbling vortex, that is, a flow rotating in the direction normal to the cylinder axis is formed when part of the intake valve is masked. Compression by the piston during the second half of the compression stroke leads to destruction of the vortex and energy cascading from the mean flow to turbulence. Instead of shrouded valves, the tumbling motion can be achieved by using directed ports [7]. It was shown [8–10] that with the appearance of the tumbling vortex in modern multivalve engines the burning rate is sped up while emissions are reduced. In addition, the lean burn limit is extended.

In the loop-scavenged two-stroke engine, fresh charges emerge from scavenge ports as multiple jets to enter the cylinder. The jets merge at the near-boost port region as rising stream, which sweeps across the cylinder head, flows down the cylinder wall, and then escapes into the exhaust port [11–16]. Thus a loop flow connecting the scavenge ports and the exhaust port is the most distinct structure during the scavenging period and is responsible for the scavenging efficiency and the performance of the engine, which had been recognized long ago [17]. By the end of the scavenging process, the loop flow is transformed into a tumbling vortex, which may persist until the end of the compression period. This tumbling vortex

can be identified in a number of numerical simulations [11, 12, 16, 18] and experimental works [19–21]. It was evidenced in the measurements conducted by Miles et al. [21] and Reddy et al. [22] that the turbulence in the cylinder is enhanced during the compression period when the tumbling vortex is strong. The calculations of Tsui and Cheng [23] showed that the turbulence enhancement can be intensified by shaping the cylinder head via increasing the head curvature. Usually, the tumbling-generated turbulence reaches its peak level at about 20° before TDC of compression, followed by a fast decay. It was observed that the squish generated by a combustion bowl gathers strength after this time and peaks within 10° before TDC [1]. After TDC, a reverse squish is quickly formed [3]. Therefore it is a good idea to combine the tumbling flow with the squish/reverse squish such that a strong bulk flow and a relatively high turbulence level can be achieved throughout the compression and early expansion period. In the present study a multidimensional calculation procedure is used to investigate the flow in a loop-scavenged two-stroke engine. The head of the engine is equipped with a nearly semispherical combustion chamber. Focus is mainly concentrated on the tumbling motion and the squish and their interaction during the compression and the early expansion periods. Also investigated are the effects of offset of the head bowl from the cylinder axis. To the authors' best knowledge, such an investigation of tumbling/squish interaction has not been done in the literature.

MATHEMATICAL MODEL

A schematic illustration of the engine configuration is shown in Figure 1. There is one exhaust port and five scavenge ports in the cylinder liner: four transfer ports (ports B and C) and one boost port (port A). The cylinder geometry is arranged in a symmetrical manner, with a symmetry plane cutting through the boost and exhaust ports. A nearly semispherical combustion chamber appears on the cylinder head. The axis of the head bowl is located in the symmetry plane and

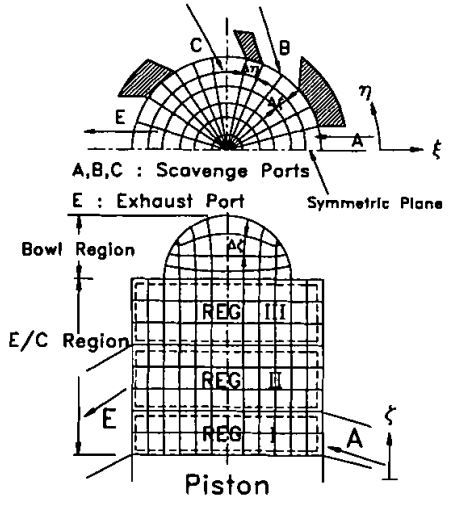

Figure 1. Illustration of the engine configuration and typical grid layout.

is either placed at the cylinder center or offset from the cylinder axis. Axisymmetrically curvilinear-orthogonal coordinates are adopted to fit the curved head of the bowl. As shown in Figure 1, the coordinate η is in the circumferential direction, and the coordinates ξ and ζ are mutually orthogonal in the constant-η plane. In this coordinate system the general transport equation for the head bowl region can be cast into the following form.

$$\frac{\partial}{\partial t}(\rho\Phi) + \frac{1}{\Delta\eta\Delta\zeta}\frac{\partial}{\partial\xi}(\Delta\eta\Delta\zeta\rho u\Phi) + \frac{\partial}{\partial\eta}(\rho v\Phi) + \frac{1}{\Delta\xi\Delta\eta}\frac{\partial}{\partial\zeta}(\Delta\xi\Delta\eta\rho w\Phi)$$
$$= \frac{1}{\Delta\eta\Delta\zeta}\frac{\partial}{\partial\xi}\left(\Delta\eta\Delta\zeta\,\Gamma_\Phi\frac{\partial\Phi}{\partial\xi}\right) + \frac{\partial}{\partial\eta}\left(\Gamma_\Phi\frac{\partial\Phi}{\partial\eta}\right)$$
$$+ \frac{1}{\Delta\xi\Delta\eta}\frac{\partial}{\partial\zeta}\left(\Delta\xi\Delta\eta\,\Gamma_\Phi\frac{\partial\Phi}{\partial\zeta}\right) + S_\Phi \tag{1}$$

where u, v, and w are the velocity components along the ξ, η, and ζ directions. Detailed expressions are referenced to Tsui and Cheng [13].

The region below the bowl is swept by the moving piston, and its volume contracts and expands in accordance with the piston motion. To comply with this feature, the grid lines in this region are allowed to move with the piston. As seen in Figure 1, this expansion/compression (E/C) region is divided into three subregions, with the two lines at the upper edges of the exhaust and scavenge ports as the interfaces. Whenever the piston moves into one subregion, the grid lines in that region are set in motion, and those in the other regions are motionless. The speed of the moving grids varies as a linear function of axial distance in the region. Grids in subregions I and II are added into or deleted from the computational domain, depending on whether the region is opened or closed at that instant. On the transverse plane perpendicular to the cylinder axis, bipolar coordinates are employed to accommodate the off-center bowl. The transport equations in this region then can be written as

$$\frac{1}{\Delta V}\frac{\partial}{\partial t}(\rho\Phi\Delta V) + \frac{1}{\Delta\eta}\frac{\partial}{\partial\xi}(\Delta\eta\rho u\Phi) + \frac{1}{\Delta\xi}\frac{\partial}{\partial\eta}(\Delta\xi\rho v\Phi) + \frac{\partial}{\partial\zeta}(\rho\hat{w}\Phi)$$
$$= \frac{1}{\Delta\eta}\frac{\partial}{\partial\xi}\left(\Delta\eta\,\Gamma_\Phi\frac{\partial\Phi}{\partial\xi}\right) + \frac{1}{\Delta\xi}\frac{\partial}{\partial\eta}\left(\Delta\xi\,\Gamma_\Phi\frac{\partial\Phi}{\partial\eta}\right) + \frac{\partial}{\partial\zeta}\left(\Gamma_\Phi\frac{\partial\Phi}{\partial\zeta}\right) + S_\Phi \tag{2}$$

where ΔV is the volume of the considered cell and $\hat{w}$ is the axial velocity relative to the moving-grid velocity. Complete equations in the E/C region can be seen in the work by Tsui and Cheng [12].

The turbulent flow in the engine is characterized by the high-Reynolds-number k-ϵ model of Launder and Spalding [24]. The wall function is used to bridge the near-wall region as boundary conditions at solid walls. Specifications of intake and exhaust velocities at the openings of the scavenge and exhaust ports are essential to the calculation. The mass fluxes through these ports are modeled by

one-dimensional orifice flow:

$$\dot{m} = \rho A C_D \sqrt{2\,\Delta P/\rho} \tag{3}$$

where ρ is the density upstream of the flow through the considered port, A denotes the area of the port opening, C_D the discharge coefficient, and ΔP the effective pressure difference between the crankcase and the cylinder for the scavenge port or the difference between the exhaust pipe and the cylinder for the exhaust port. Given pressures in the crankcase and outside the exhaust port, the mass fluxes can be determined through overall mass and energy balances in the cylinder. The velocity, derived from the mass flow rate, is then assumed to be uniformly distributed over the opening area. In the previous study of Tsui and Cheng [13], three sets of pressure data were adopted to examine the flow during the scavenge period. The set used in this study corresponds to the set of the lowest flow rate.

Following Gosman and Johns [3], the grids in the bowl are generated by solving two-dimensional inverse Laplace equations. Governing equation are discretized using the finite volume method. The coupling between the continuity and momentum equations and that between the k and ϵ equations are tackled by the EPISO algorithm [12, 13, 23], which adopts the concept of predictor-corrector. Since the flow in the cylinder is subject to a bulk temporal change in pressure, temperature, and density due to piston displacement, a global adjustment is conducted in the algorithm such that the overall mass and energy in the cylinder are conserved. Details about the solution procedure can be found in the cited references.

RESULTS AND DISCUSSION

The solution method described above has been validated in the previous studies [13, 23]. In the first study [13] the pressures in the crankcase and outside the exhaust port, measured by Fansler and French [25], were specified at the open boundaries of the scavenge and exhaust ports, respectively. Then the mass fluxes through these ports, estimated according to Eq. (3), were imposed as boundary conditions for the in-cylinder flow calculation. The variation of the predicted in-cylinder pressure during the scavenging period was quite similar to the measurements of Fansler and French and the predictions of Amsden et al. [26]. In the calculation of Amsden et al. the computational domain covered the cylinder as well as the passages of the scavenge ports and the exhaust port. Also compared were the evolution of the mass of the fresh charge captured in the cylinder and the mass of residual gas left in the cylinder from the previous cycle. It was shown that there existed strong oscillations for the masses of the fresh charge and the residual gas in the early scavenging period using the present method, but not in the study of Amsden et al. This was due to the fact that with the present calculation procedure the effects of pressure wave in the port passages were ignored, i.e., the flow inertia was not accounted for. However, the total mass in the cylinder was not much affected. In the late scavenging period the results of the two predictions were in good agreement. As a consequence, the differences in the prediction of trapping

efficiency and scavenging efficiency were within 5%. Validation of the solution method could also be found in another study [23], in which good agreement with experimental data in terms of scavenging efficiency as well as scavenge ratio for a number of scavenging flow rates was observed.

In the following tests, five cylinder head arrangements (Figure 2) are under consideration. In the first three cases a nearly semispherical bowl is placed on the cylinder head. The bowl is displaced toward the exhaust port side in case I and toward the boost port side in case III, while the bowl is centrally located in case II. The results for the engines equipped with a flat head (case IV) and a curved head (case V) are also presented in the following for the sake of comparison. In case V the radius of head curvature is 70 mm. Details of the operating characteristics and engine specifications are given in Table 1. Because of the symmetric arrangement, only half a cylinder volume is considered in the computation. Calculations commence at the exhaust port opening (EPO) and end at 400° crank angle (CA).

Grid sensitivity tests have been conducted using 64,800, 92,500, and 127,050 nodal points in the E/C region and 25,920, 42,550, and 64,680 nodal points in the head region for case I. As shown in Figure 3, the variation of the kinetic energy of mean flow, averaged over the entire cylinder, with respect to the change of grid spacing was nearly negligible, whereas the turbulence had larger dependence on the grid spacing. However, the deviation in terms of cylinder-averaged turbulence intensity was less than 7% for the two fine meshes. It is therefore expected that the finest mesh, with a $42 \times 55 \times 55$ ($r \times \theta \times z$) grid in the E/C region and a $28 \times 55 \times 42$ grid in the bowl region, is adequate to resolve the flow characteristics. This mesh is denser than those employed in previous studies [13, 23].

In order to illustrate the flow fields, velocity vectors and turbulence intensity contours in the symmetry plane at a number of crank angles are presented. To avoid clustering, the velocity vectors are plotted every other point along the grid lines. The turbulence intensity is normalized by the mean piston speed ($\overline{V}_p = 7.5$ m/s). Focus is concentrated on the compression and early expansion. The flow fields are shown in Figures 4 and 5 for cases I and III, respectively. The flow characteristics of case II lie between cases I and III, and those for cases IV and V are similar to the results illustrated by Tsui and Cheng [23]. During the scavenging

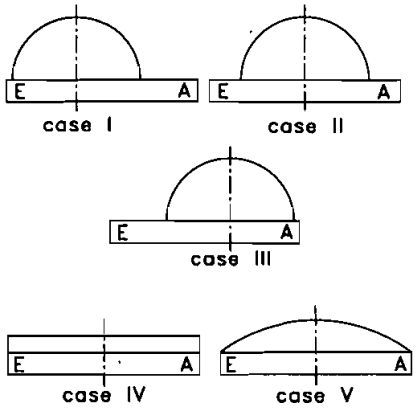

Figure 2. Illustration of test cases.

Table 1. Engine specifications

Parameter	Value
Engine speed	3000 rpm
Cylinder bore	74.0 mm
Stroke	75.0 mm
Bumping clearance	0.85 mm
Bowl diameter	50.0 mm
Bowl depth	23.5 mm
Bowl offset	0 or $\pm$11.4 mm
Volume of bowl	29.86 mm^3
Effective compression ratio	7.3
Exhaust port opening	100° CA
Exhaust port closing	260° CA
Scavenge port opening	125° CA
Scavenge port closing	235° CA

CA, crank angle.

period, the airstreams emerging from scavenge ports coalesce at the region near the boost port to form a rising flow, which sweeps across the cylinder head and flows downward to run out of the cylinder from the exhaust port. This scavenging flow is transformed into a tumbling vortex flow after the scavenge and exhaust ports are closed. As shown in the figures, the vortex structure at 270° CA is well constructed in case III, and that for case I is greatly distorted because of the offset of the head bowl away from the boost port. By 300° CA, the situation is more pronounced. Squish (radially inward flow in the cylinder gap) starts to build up after this crank angle. Figure 6 presents the mean squish velocities at the edge of the bowl, averaged over the clearance gap, obtained in the present calculations and by the simple theory of Fitzgeorge and Allison [1]. Good agreement is evident in the figure. The peak value of the squish velocity is reached at about 10 BTDC, followed by a quick decline. The bowl offset gives rise to variation of squish around the bowl periphery, with stronger squish produced on the side of the bowl opposite the direction of offset. The penetration of the squish toward the bowl axis on the boost port side is hindered in case I because its flow direction is against the tumbling vortex flow there, while the tumbling flow helps increase the squish penetration on the exhaust port side in case III. As a consequence, at 340° CA the tumbling vortex dominates the flow pattern in the bowl, with its rotating center being close to the exhaust port, and an insignificant secondary vortex, rotating in a direction counter to the tumbling vortex, is formed above the squish entrance region on the boost port side in the former case.

The squish is arrested at TDC, and the air in the bowl is getting ready to rush out to fill the increased clearance between the head shoulder and the piston crown because of the descent of the piston. As seen in Figure 6, maximum reverse squish is achieved at about 10° ATDC. The results at 400° CA, shown in Figures 4*a* and 5*a*, reveal that the vortices in the bowl have disappeared under the actions of turbulence stresses and the stretching of the fluid and a torroidal vortex is formed in the squish region.

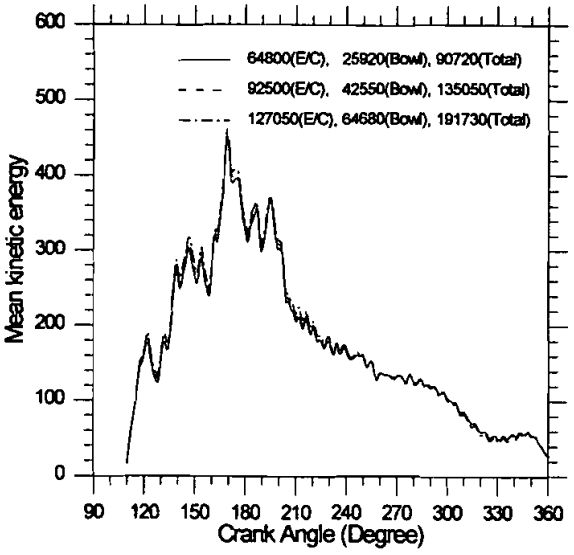

(*a*)

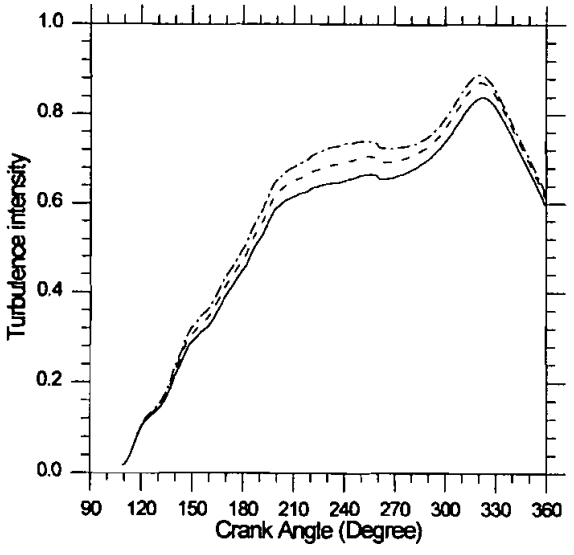

(*b*)

Figure 3. Grid refinement test for case I: (*a*) mean kinetic energy and (*b*) turbulence intensity.

The peak turbulence level shown in Figure 4*b* for case I is increased from 270° CA to 300° CA, followed by a decrease at 340° CA. As for case III (Figure 5*b*), the peak value monotonically decreases with the crank angle. It is also interesting to note that the peak region in case I during the early compression period is located close to the cylinder head shoulder, where the tumbling vortex is greatly

distorted, resulting in large shear stresses. More about this point will be addressed below. In the expansion period, turbulence is generated in the squish region due to the reverse squish, but the turbulence level in the bowl is largely attenuated, as seen at 400° CA.

The evolution of cylinder-averaged kinetic energy of the mean flow during the considered period is shown in Figure 7. Compared with case III, cases I and II have a higher level of mean flow energy in the initial compression stage, but the higher decay rate starting at the midcompression period for these cases leads to a lower level of energy thereafter. It is apparent that there exists a mean flow energy augmentation just before and after TDC, which is obviously due to the squish and reverse squish flows.

The evolution of cylinder-averaged turbulence intensity normalized by the mean piston speed is illustrated in Figure 8. In cases I and II the turbulence level shows little change before 300° CA. It is followed by a large intensification and reaches its peak at about 320° CA. Afterward, turbulence in the cylinder quickly decays. The turbulence augmentation in the period 280° < CA < 320° is attributed

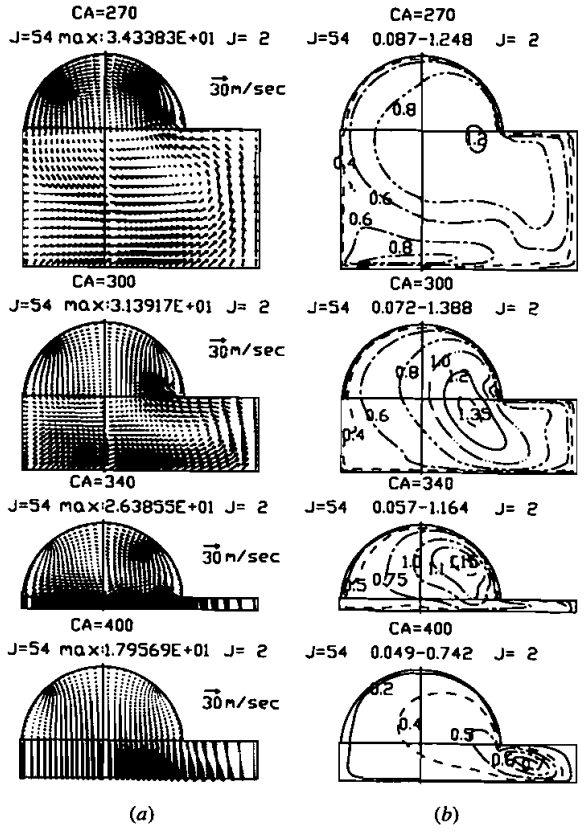

Figure 4. (*a*) Mean flow field and (*b*) turbulence intensity field for case I.

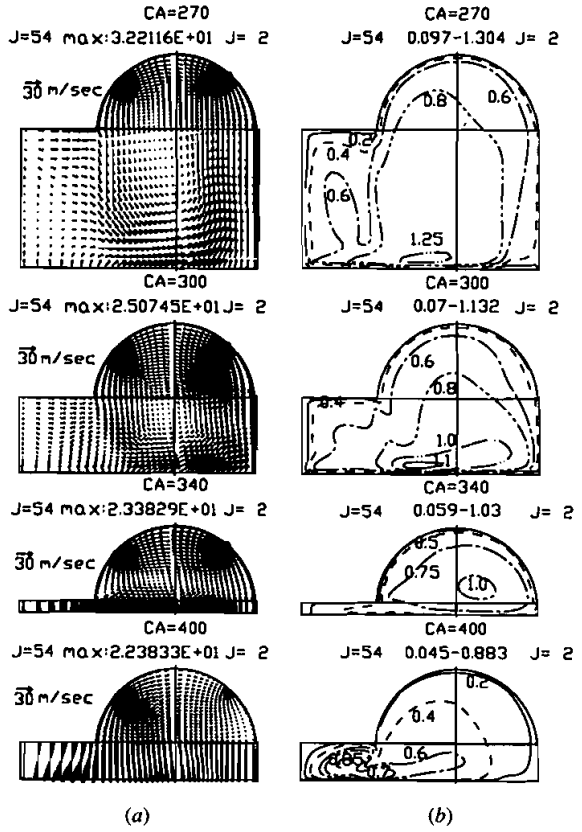

Figure 5. (*a*) Mean flow field and (*b*) turbulence intensity field for case III.

to the compression of the tumbling vortex [23]. However, the augmentation phenomenon is insignificant in case III. Examination of the curves shown in Figures 7 and 8 reveals that when turbulence is largely intensified for cases I and II, the mean flow energy decays rapidly, and vice versa for case III. Although the turbulence level for case III is lower throughout most of the compression period than those for cases I and II, it has larger turbulence by the end of compression and in the expansion stage because of the stronger mean flow, as seen in Figure 7.

It was shown in the previous study [23] that without the bowl, i.e., with a flat or a curved head as incorporated in cases IV or V, the tumbling vortex dominates the flow structure throughout the entire compression stroke. The well-organized vortex of case V leads to the greatest augmentation of turbulence before starting decay. However, the squish and reverse squish, taking place in the late compression and early expansion, enhance the mean flow energy, which in turn, reduces the attenuation of turbulence after augmentation in the bowl cases. At 400° CA the average turbulence levels are $0.38\overline{V}_P$, $0.37\overline{V}_P$, $0.43\overline{V}_P$, $0.26\overline{V}_P$, and $0.30\ \overline{V}_P$ for cases I–V.

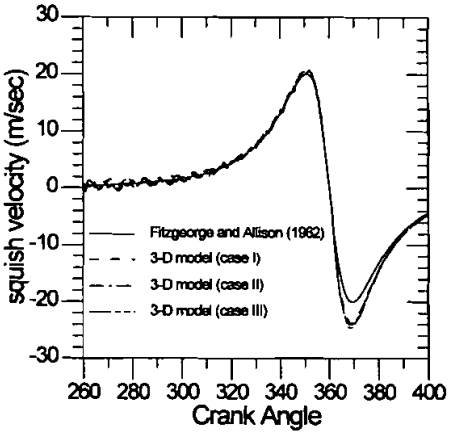

Figure 6. Evolution of mean squish velocity at the bowl periphery.

To identify the mechanism responsible for the behavior of the turbulence evolution, the temporal variations of the integrals over the cylinder volume of the total turbulence generation and dissipation components of the turbulence energy equation for the bowl cases are exhibited in Figure 9. The rate of change of turbulence level in the cylinder is dependent upon the difference between total production and dissipation. The turbulence enhancement seen in Figure 8 occurs roughly in the period between the two crossovers of the two curves for the total generation and dissipation during compression. The turbulence production surpassing the dissipation is of small magnitude and restricted in a narrow period in case III, giving rise to a flat turbulence evolution curve seen in Figure 8. Also included in Figure 9 are the individual contributions to turbulence production due to shear stresses and compression. The compression production is nearly the same for each case because it is directly related to the volumetric change rate of the cylinder volume. Maximum dilatation rate occurs at about 330° CA. The shear production is the larger of the two contributions, and there exist large differences in this production area among the three cases. Three peaks can be identified in the curve of the shear production, the first being caused by compression of the tumbling

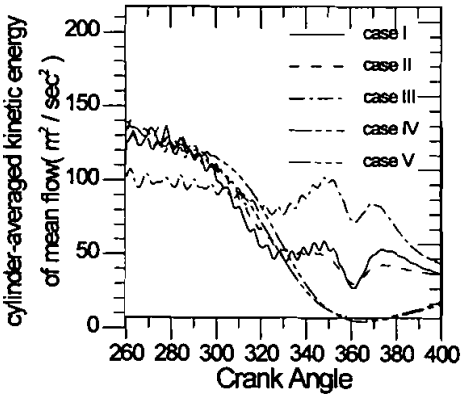

Figure 7. Temporal variation of mean kinetic energy.

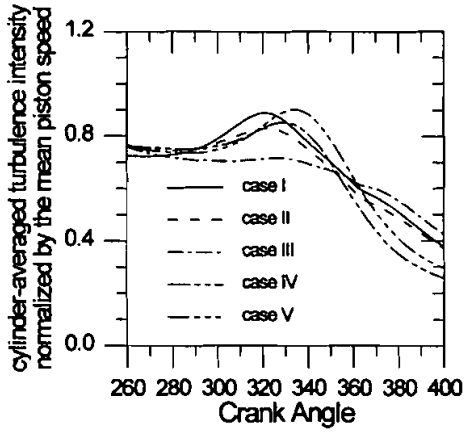

Figure 8. Temporal variation of turbulence intensity.

vortex and the other two reflecting the effects of squish and reverse squish. However, in the squish and reverse squish periods the overall turbulence levels decay monotonically because the dissipation has surpassed the total production. However, the increased shear production does help narrow the difference of the two, leading to a lower turbulence decay rate for the bowl cases when compared with the flat and curved head cases.

Figures 10 and 11 depict the temporal variations of the integrals of turbulence production and dissipation over the E/C and bowl regions separately for cases I and III, respectively. It can be seen that the total production is smaller than

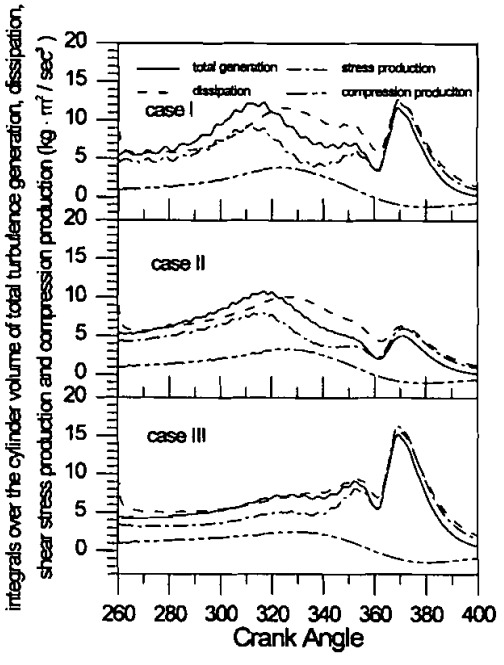

Figure 9. Temporal variation of integrals over the cylinder volume of total turbulence generation, dissipation, shear stress production, and compression production for cases I, II, and III.

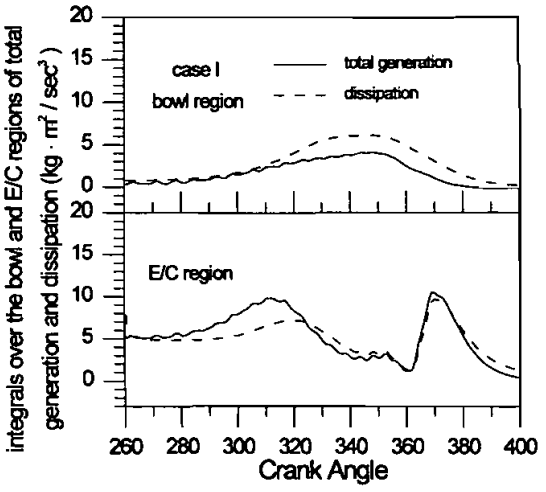

Figure 10. Temporal variation of integrals over the bowl and E/C regions of total generation and dissipation for case I.

the dissipation throughout the compression and expansion stage in the bowl, irrespective of its position. The compression of the tumbling flow in the E/C region is responsible for the turbulence augmentation. It can be seen in Figure 4*a* that the tumbling flow in the E/C region is greatly distorted by the head shoulder at 270° and 300° CA for case I, creating large shear stresses and producing large turbulence in the region near the shoulder. The high-turbulence zone then migrates into the bowl via vortex transport. It can also be seen in Figure 5*a* that at

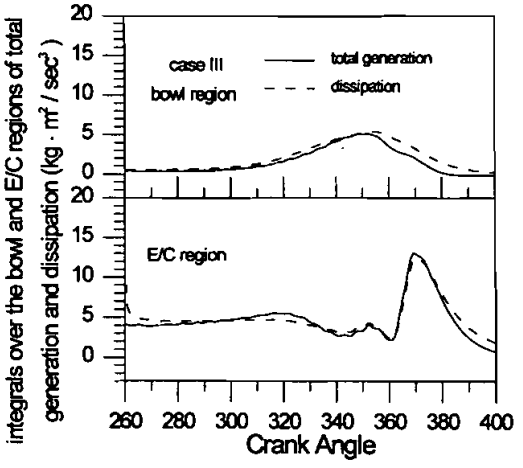

Figure 11. Temporal variation of integrals over the bowl and E/C regions of total generation and dissipation for case III.

270° and 300° CA the vortex formed in case III is restricted in the cylinder under the bowl head while the flow in the E/C region between the head shoulder and piston crown is nearly in the radially inward direction, apart from that near the piston. Since the axial dimension of the vortex is increased by the appearance of the head bowl, the enhancement of shear stress, and thus turbulence production due to piston compression is less effective. At the stage of expansion close to TDC, the strong reverse squish results in large turbulence production, which overrides the dissipation in the E/C region. Therefore, as seen in Figures 4*b* and 5*b*, high turbulence is generated in the squish region. However, the overall turbulence level in the entire cylinder continuously attenuates, as observed in Figure 8.

CONCLUSIONS

On the basis of the above results, the main findings regarding the flow during compression and early expansion periods in a loop-scavenged two-stroke engine, which incorporates a centrally located or an off-center head bowl, are summarized as follows.

1. The tumbling vortex is the most prominent flow pattern in the cylinder before late compression. For cases with the bowl offset toward the exhaust port (case I) and the centrally located bowl (case II), compression of the distorted tumbling flow in the E/C region leads to augmentation of turbulence in the period from 280° to 320° CA. However, the turbulence enhancement is not significant for the case with the bowl displaced toward the boost port (case III). This is mainly ascribed to the fact that the axial dimension of the vortex is increased by the piston bowl.
2. The squish gradually becomes important as TDC is approached in the late compression period. Maximum squish velocity is achieved at about 10° BTDC. The penetration of the squish flow is obstructed on the boost port side and enhanced on the exhaust port side by the tumbling vortex. The tumbling vortex is still the dominant flow pattern in the head bowl. Despite the squish flow, resulting in increased shear effects, turbulence continuously decays in this period.
3. In the early expansion stage the tumbling vortex in the bowl disappears, and the reverse squish creates a torroidal vortex in the squish region. Although locally, high turbulence is generated in the squish region, the overall level of turbulence in the entire cylinder volume continues to decay.
4. Although the turbulence augmentation of case III is the least effective, it has the strongest mean flow and the lowest turbulence decay rate in the late compression and expansion periods. This leads to the highest turbulence levels after TDC for this case.
5. Compared with the cases without head bowl, especially the case with a curved head, the turbulence augmentation in the bowl cases is less significant. However, squish and reverse squish generated in these cases give rise to a lower decay rate and thus higher turbulence levels in the later period.

REFERENCES

1. D. Fitzgeorge and J. L. Allison, Air Swirl in a Road-Vehicle Diesel Engine, *Inst. Mech. Eng. Proc. Automobile Div.*, no. 4, pp. 151–168, 1962.
2. G. C. Davis and J. C. Kent, Comparison of Model Calculations and Experimental Measurements of the Bulk Cylinder Flow Processes in a Motored PROCO Engine, SAE Paper 790290, 1979.
3. A. D. Gosman and R. J. R. Johns, Development of a Predictive Tool for In-Cylinder Gas Motion in Engines, SAE Paper 780315, 1978.
4. C. Arcoumanis, A. F. Bicen, and J. H. Whitelaw, Squish and Swirl-Squish Interaction in Motored Model Engines, *ASME J. Fluids Eng.*, vol. 105, pp. 105–112, 1983.
5. S. H. El Tahry, A Numerical Study on the Effects of Fluid Motion at Inlet-Valve Closure on Subsequent Fluid Motion in a Motored Engine, SAE Paper 820035, 1982.
6. A. D. Gosman, Y. Y. Tsui, and C. Vafidis, Flow in a Model Engine with a Shrouded Valve—A Combined Experimental and Computational Study, SAE Paper 850498, 1985.
7. C. Arcoumanis, Z. Hu, C. Vafidis, and J. H. Whitelaw, Tumbling Motion: A Mechanism for Turbulence Enhancement in Spark-Ignition Engines, SAE Paper 900060, 1990.
8. O. Hadded and I. Denbratt, Turbulence Characteristics of Tumbling Air Motion in Four-Valve S. I. Engines and Their Correlation with Combustion Parameters, SAE Paper 910478, 1991.
9. S. Omori, K. Iwachido, M. Motomochi, and O. Hirako, Effect of Intake Port Flow Pattern on the In-Cylinder Tumbling Air Flow in Multi-Valve SI Engines, SAE Paper 910477, 1991.
10. H. Endres, H. J. NeuBer, and R. Wurms, Influence of Swirl and Tumble on Economy and Emissions of Multivalve SI Engines, SAE Paper 920516, 1992.
11. B. Ahmadi-Befrui, W. Brandstatter, and H. Kratochwill, Multidimensional Calculation of the Flow Processes in a Loop-Scavenged Two-Stroke Cycle Engine, SAE Paper 890841, 1989.
12. Y.-Y. Tsui and H.-P. Cheng, Flow Calculation in a Loop-Scavenged Two-Stroke Motored Engine, *Int. J. Numer. Methods Heat Fluid Flow*, vol. 4, pp. 249–267, 1994.
13. Y.-Y. Tsui and H.-P. Cheng, Scavenging Process in Loop-Scavenged Two-Stroke Engines, *J. Chinese Soc. Mech. Eng.*, vol. 17, no. 15, pp. 465–473, 1996.
14. Y.-G. Lai, A. J. Przekwas, and R. L. T. Sun, Three-Dimensional Computation of the Scavenging Flow Process in a Motored Two-Stroke Engine, SAE Paper 930499, 1993.
15. N. R. McKinley, R. G. Kenny, and R. Fleck, CFD Prediction of a Two-Stroke, In-Cylinder Steady Flow Field: An Experimental Validation, SAE Paper 940399, 1994.
16. H. Hori, T. Ogawa, and T. Kuriyama, CFD In-Cylinder Flow Simulation of an Engine and Flow Visualization, SAE Paper 950288, 1995.
17. A. Jante, Scavenging and Other Problems of Two-Stroke Cycle Spark-Ignition Engines, SAE Paper 680468, 1968.
18. L. Yu, T. Campbell, and W. Pollock, A Simulation Model for Direct Fuel Injection of Two-Stroke Gasoline Engines, SAE Paper 970366, 1997.
19. T. Sato and M. Nakayama, Gasoline Direct Injection for a Loop-Scavenged Two-Stroke Cycle Engine, SAE Paper 871690, 1987.
20. T. Ohira, Y. Ikeda, K. Kakemizu, and T. Nakajima, In-Cylinder Flow Measurement and Its Application for Cyclic Variation Analysis in a Two-Stroke Engine, SAE Paper 950224, 1995.
21. P. C. Miles, R. M. Green, and P. O. Witze, In-Cylinder Gas Velocity Measurements Comparing Crankcase and Blower Scavenging in a Fired Two-Stroke Cycle Engine, SAE Paper 940401, 1994.
22. K. V. Reddy, V. Ganesan, and K. V. Gopalakrishnan, Under the Roof of the Cylinder Head—An Experimental Study of the In-Cylinder Air Movement in a Two-Stroke Spark Ignition Engine, SAE Paper 860166, 1986.

23. Y.-Y. Tsui and H.-P. Cheng, Tumbling Flow in Loop-Scavenged Two-Stroke Engines, *ASME J. Fluids Eng.*, vol. 117, pp. 628–632, 1995.
24. B. E. Launder and D. B. Spalding, The Numerical Computation of Turbulent Flow, *Comput. Methods Appl. Mech. Eng.*, vol. 3, pp. 269–289, 1974.
25. T. D. Fansler and D. T. French, The Scavenging Flow Field in a Crankcase-Compression Two-Stroke Engine—A Three-Dimensional Laser-Velocimetry Survey, SAE Paper 920417, 1992.
26. A. A. Amsden, P. J. O'Rourke, T. D. Butler, K. Meintjes, and T. D. Fansler, Comparisons of Computed and Measured Three Dimensional Velocity Fields in a Motored Two-Stroke Engine, SAE Paper 920418, 1992